analytical chemistry

Article

pubs.acs.org/ac

Combining Raman and FT-IR Spectroscopy with Quantitative Isotopic Labeling for Differentiation of *E. coli* Cells at Community and Single Cell Levels

Howbeer Muhamadali,[†,‡] Malama Chisanga,[†,‡,§] Abdu Subaihi,[‡] and Royston Goodacre*[,‡]

[‡]School of Chemistry, Manchester Institute of Biotechnology, University of Manchester, Manchester, United Kingdom

[§]School of Mathematics and Natural Sciences, Department of Chemistry, Copperbelt University, Kitwe, Zambia

Supporting Information

ABSTRACT: There is no doubt that the contribution of microbially mediated bioprocesses toward maintenance of life on earth is vital. However, understanding these microbes *in situ* is currently a bottleneck, as most methods require culturing these microorganisms to suitable biomass levels so that their phenotype can be measured. The development of new culture-independent strategies such as stable isotope probing (SIP) coupled with molecular biology has been a breakthrough toward linking gene to function, while circumventing *in vitro* culturing. In this study, for the first time we have combined Raman spectroscopy and Fourier transform infrared (FT-IR) spectroscopy, as metabolic fingerprinting approaches, with SIP to demonstrate the quantitative labeling and differentiation of *Escherichia coli* cells. *E. coli* cells were grown in minimal medium with fixed final concentrations of carbon and nitrogen supply, but with different ratios and combinations of $^{13}C/^{12}C$ glucose and $^{15}N/^{14}N$ ammonium chloride, as the sole carbon and nitrogen sources, respectively. The cells were collected at stationary phase and examined by Raman and FT-IR spectroscopies. The multivariate analysis investigation of FT-IR and Raman data illustrated unique clustering patterns resulting from specific spectral shifts upon the incorporation of different isotopes, which were directly correlated with the ratio of the isotopically labeled content of the medium. Multivariate analysis results of single-cell Raman spectra followed the same trend, exhibiting a separation between *E. coli* cells labeled with different isotopes and multiple isotope levels of C and N.

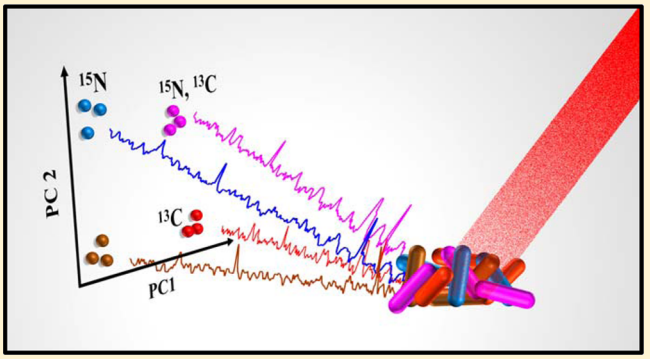

Since the first exploration steps into the microbial world through the invention of the early light microscopes,[1] the science of microbiology has come a long way. The steady stream of scientific discoveries in parallel with technological advancements have provided us with a deeper understanding of the biology of bacteria and what goes on inside the cell at different levels, giving rise to various fields of research such as genomics, transcriptomics, proteomics, and metabolomics.[2,3]

Despite the above accomplishments, most microorganisms (>99%) remain uncultured under laboratory conditions,[4] which holds back our understanding of the functional roles of many bacterial communities. Therefore, culture-independent tools such as metagenomics[5−9] and single-cell based technologies[10−12] have been explored and successfully applied to the field of microbiology to circumvent the need for culturing.

Although vast amount of metagenomics data sets have provided us with a wealth of knowledge on constituents of different microbial communities, in most cases this approach is still unable to elucidate clearly the link between gene and function with respect to the role of the different members within a community. This is due to the fact that the presence of a gene does not simply reflect its use in the cell, even if an active transcription and translation is demonstrated, the encoded enzyme could still be inactive and lack any biological function. However, since the metabolome[13] is considered the downstream product of genome, transcriptome, and proteome, the application of metabolomic in parallel to genomic approaches may provide a clearer picture of the phenotype and function of a biological system.[14]

During the past two decades the application of Raman microspectroscopy as a metabolic fingerprinting tool, has revolutionized the fields of microbial ecology and environmental microbiology by allowing the *in situ* exploration of microbes at single-cell level.[11,12,15] The Raman scattering effect is generally described as the inelastic scattering of photons (usually from an intense light source like a laser) by which the scattered photons are at a higher (anti-Stokes) or lower (Stokes) energy state in comparison to the incident photons. This energy shift which is mainly caused by the interaction of photons with the chemical bond vibrations of the investigated sample, provides detailed insight in to the biochemical composition and structural

Received: March 6, 2015
Accepted: April 1, 2015
Published: April 1, 2015

DOI: 10.1021/acs.analchem.5b00892
Anal. Chem. 2015, 87, 4578−4586

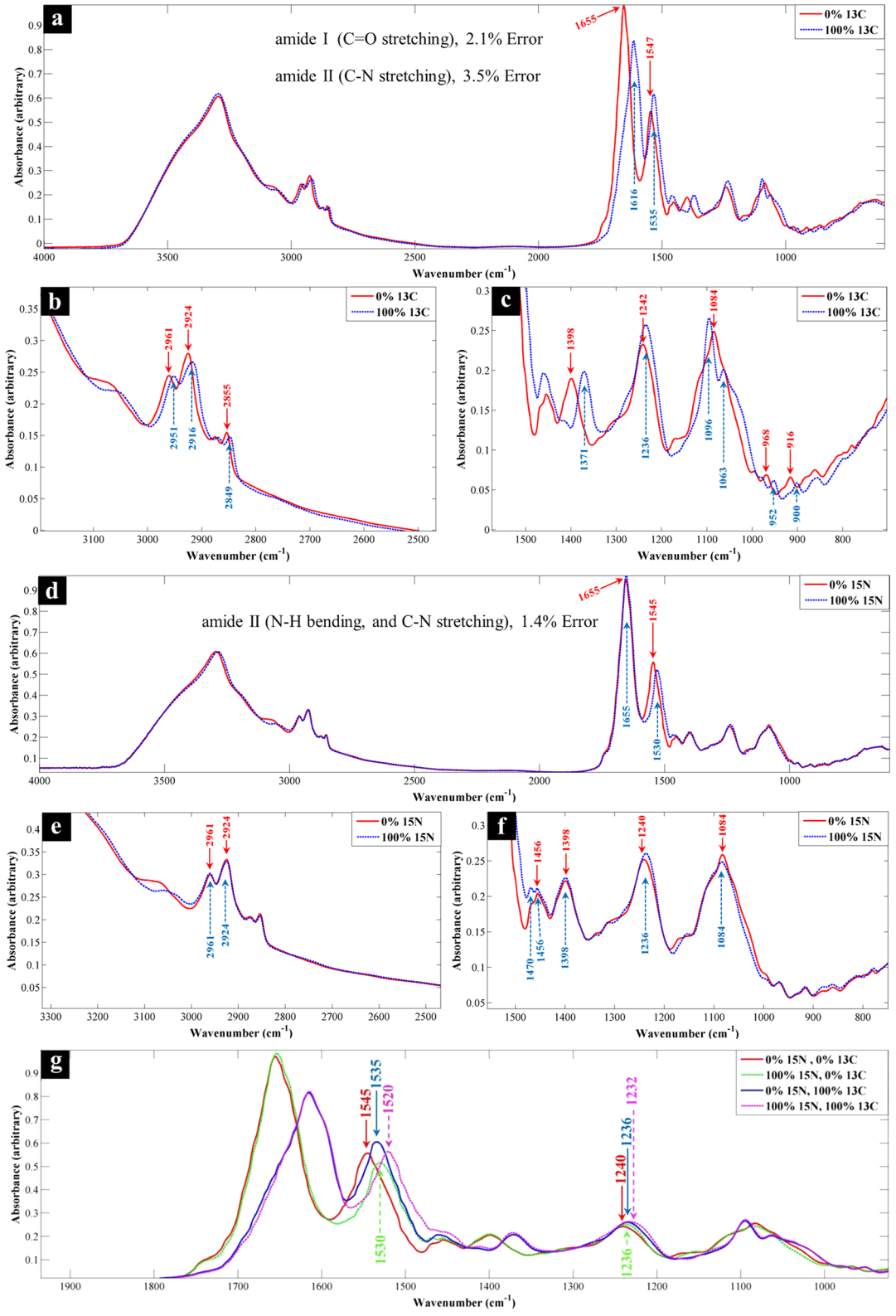

Figure 1. FT-IR spectra of *E. coli* cells grown with unlabeled substrates (red line) or ^{13}C labeled (dashed blue line) glucose as the sole carbon source (a–c), ^{15}N labeled (dashed blue line) ammonium chloride as the sole nitrogen source (d–f), or combinations of labeled glucose and ammonium chloride (g). (a, d) illustrates the complete FT-IR spectra, while (b, e and c, f) shows enlarged view of two different spectral areas, corresponding band assignments are provided in Table S1. The spectra presented above are average of 18 replicates. The errors of the shifted peaks are calculated according to eq 3. In (g), labeled (^{13}C, ^{15}N) and unlabeled (^{12}C, ^{14}N) glucose and ammonium chloride are used as the sole carbon and nitrogen sources, respectively, and the legend highlights the colors used for plotting.

properties of the sample, such as proteins, nucleic acids, lipids, polysaccharides, and carbohydrates.[16,17]

As a complementary vibrational spectroscopy tool Fourier transform infrared (FT-IR) spectroscopy[18] has also been proven

DOI: 10.1021/acs.analchem.5b00892
Anal. Chem. 2015, 87, 4578–4586

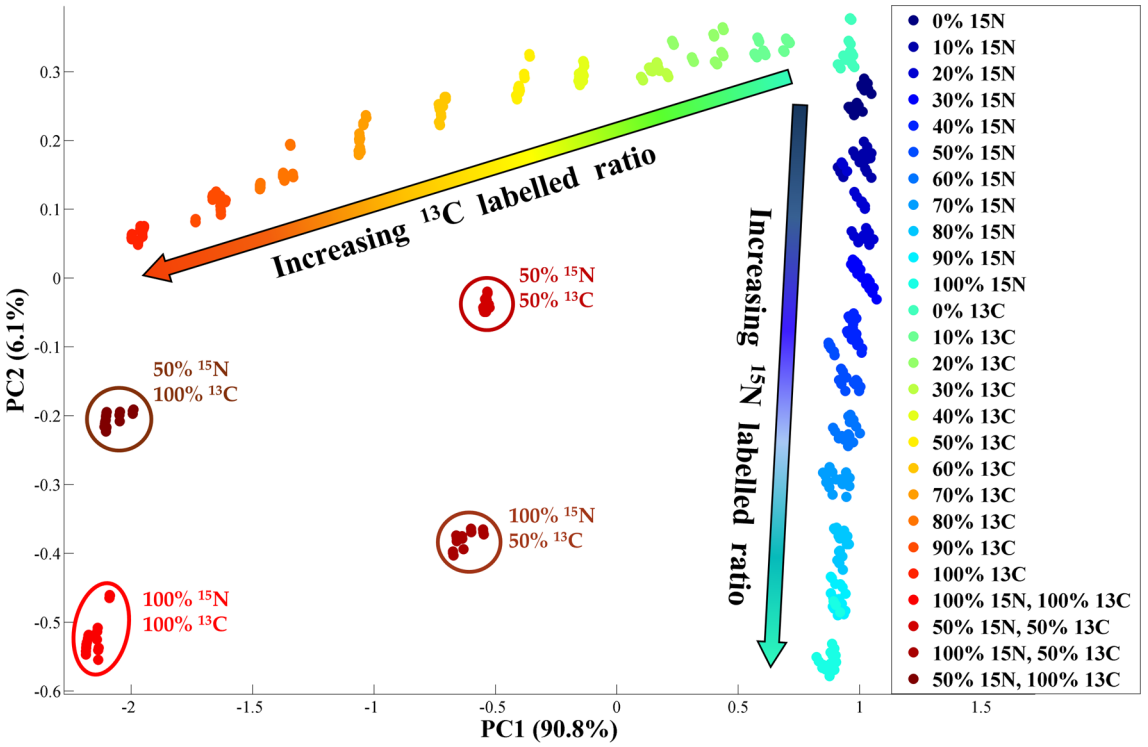

Figure 2. PCA scores plot of preprocessed FT-IR spectra of *E. coli* cells grown using various ratios and combinations of labeled (^{13}C, ^{15}N) and unlabeled (^{12}C, ^{14}N) glucose and ammonium chloride. The arrows indicate the increasing ratios of the labeled substrates.

valuable for (bio)chemical investigation of microbial samples in a wide range of areas within the field of microbiology, including medical,[19−21] food,[22,23] and environmental.[24−26] However, unlike Raman scattering which is based on the inelastic scattering of light caused by the changes in polarizability of the molecule, FT-IR measures the absorption of the infrared light by the sample due to changes in the dipole moment of the molecule.[27]

Several recent studies have successfully demonstrated the applications of combining stable isotope probing (SIP) with Raman microspectroscopy for *in situ* analysis of microbial communities in terms of identification[12,28] and function.[29−31] However, to date these have mainly used 100% substrate labeling which does not indicate how much of the heavy isotope has been incorporated into the cell's biochemistry, which may aid understanding of how an organism consumes different carbon and/or nitrogen sources *in situ*.

In this study we have employed Raman and FT-IR spectroscopy combined with SIP and multivariate statistical analysis techniques, for quantitative labeling and characterization of *E. coli* cells grown on different ratios of isotopically labeled ^{13}C-glucose (U−^{13}C; all six carbons are labeled) and ^{15}N-ammonium chloride, both at community and single cell level. Our results demonstrate the potential applications of this strategy as a quantitative approach for microbial differentiation, which may provide a better understanding to the role of different microbial community members toward various microbially mediated bioprocesses.

EXPERIMENTAL METHODS

Growth Conditions. All chemicals were purchased from Fisher (Fischer Scientific, U.K.) unless otherwise stated. *E. coli* K-12 MG1655 was grown on minimal medium[32] supplemented with total of 5 g/L of varying ratios of ^{12}C- and ^{13}C-glucose (99 atom % homogeneously labeled from Sigma-Aldrich, U.K.) as the single carbon source, and 1 g/L of varying ratios of ^{14}N and ^{15}N-NH_4Cl (98 atom % homogeneously labeled; Sigma-Aldrich, U.K.) as the single nitrogen source (Table S1). Samples were incubated as 1.5 mL aliquot replicates (n = 6) in sterile 24-well plates (Greiner Bio-one, U.K.) for 15 h at 37 °C with 170 rpm shaking in a Multitron standard shaker incubator (INFORS-HT Bottmingen Switzerland). All plates were sealed using sterile Breathe-Easy sealing membranes (Sigma-Aldrich, U.K.) to reduce potential evaporation and sample loss during the incubation period.

Sample Preparation. After the incubation period, 1.3 mL aliquots from each of the samples were transferred to a 2 mL microcentrifuge tube and centrifuged for 10 min at 5000 *g* using a benchtop Eppendorf Microcentrifuge 5424R (Eppendorf Ltd., Cambridge, U.K.). The supernatant was discarded and the collected biomass was washed twice using 1 mL of sterile saline solution (0.9% NaCl) following the above centrifugation parameters. The washed biomass was resuspended in 70 μL of the saline solution and kept at −80 °C until further analysis.

FT-IR Analysis. A total of 20 μL of the washed cell samples were spotted onto a prewashed 96-well FT-IR silicon plate and heated to dryness in a 55 °C oven. FT-IR spectra were obtained in transmission mode, on a Bruker Equinox 55 infrared spectrophotometer (Bruker Optics Ltd., Coventry, U.K.). A total of 64 spectral scans were coadded and averaged for each sample between the 4000−600 cm^{-1} range with 4 cm^{-1} resolution.[33] All collected spectra were scaled using the extended multiplicative signal correction method (EMSC),[34] and the CO_2 vibrations (2400−2275 cm^{-1}) were removed and filled with a trend, before conducting any multivariate data analysis.

Raman Analysis. For bulk biomass analysis 2 μL of the washed cell samples were transferred onto prewashed calcium fluoride (CaF_2) disks and air-dried in a desiccator. Raman spectra were measured using a Renishaw inVia Raman microscope

DOI: 10.1021/acs.analchem.5b00892
Anal. Chem. 2015, 87, 4578−4586

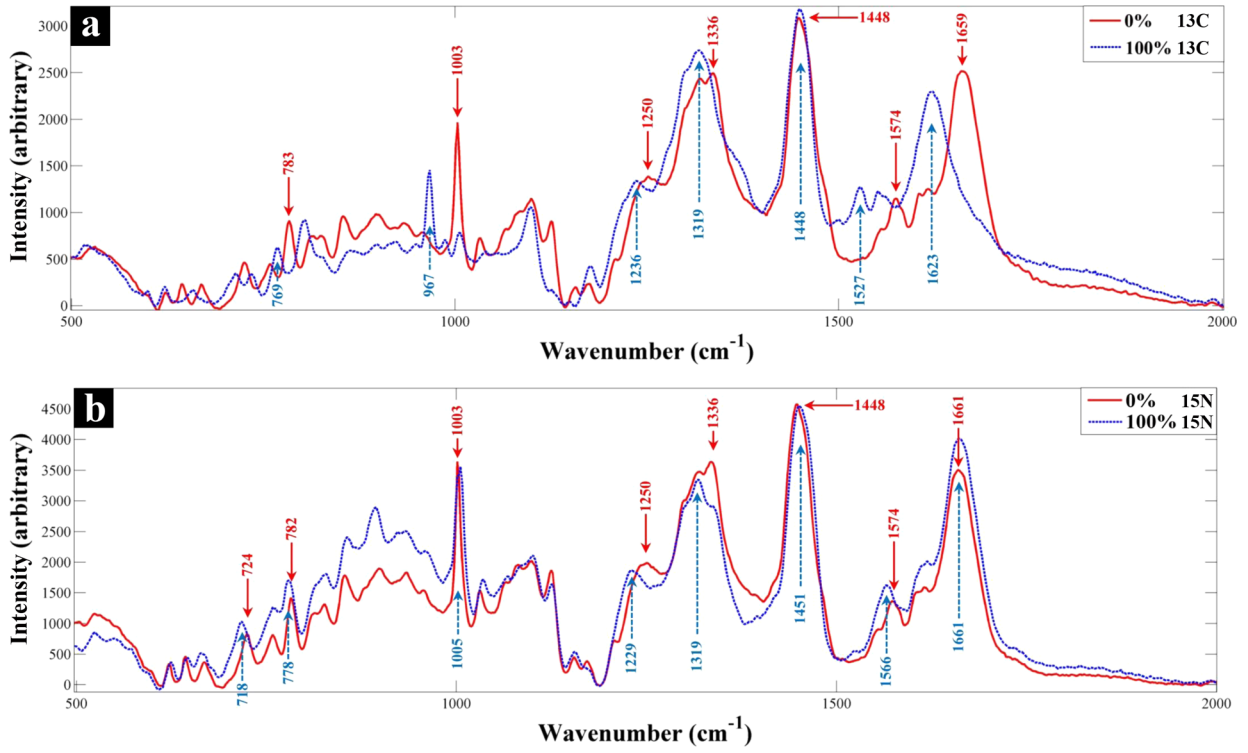

Figure 3. Raman spectra of *E. coli* cells grown on (a) labeled (^{13}C) and unlabeled (^{12}C) glucose and (b) labeled (^{15}N) and unlabeled (^{14}N) ammonium chloride as the sole carbon and nitrogen sources, respectively.

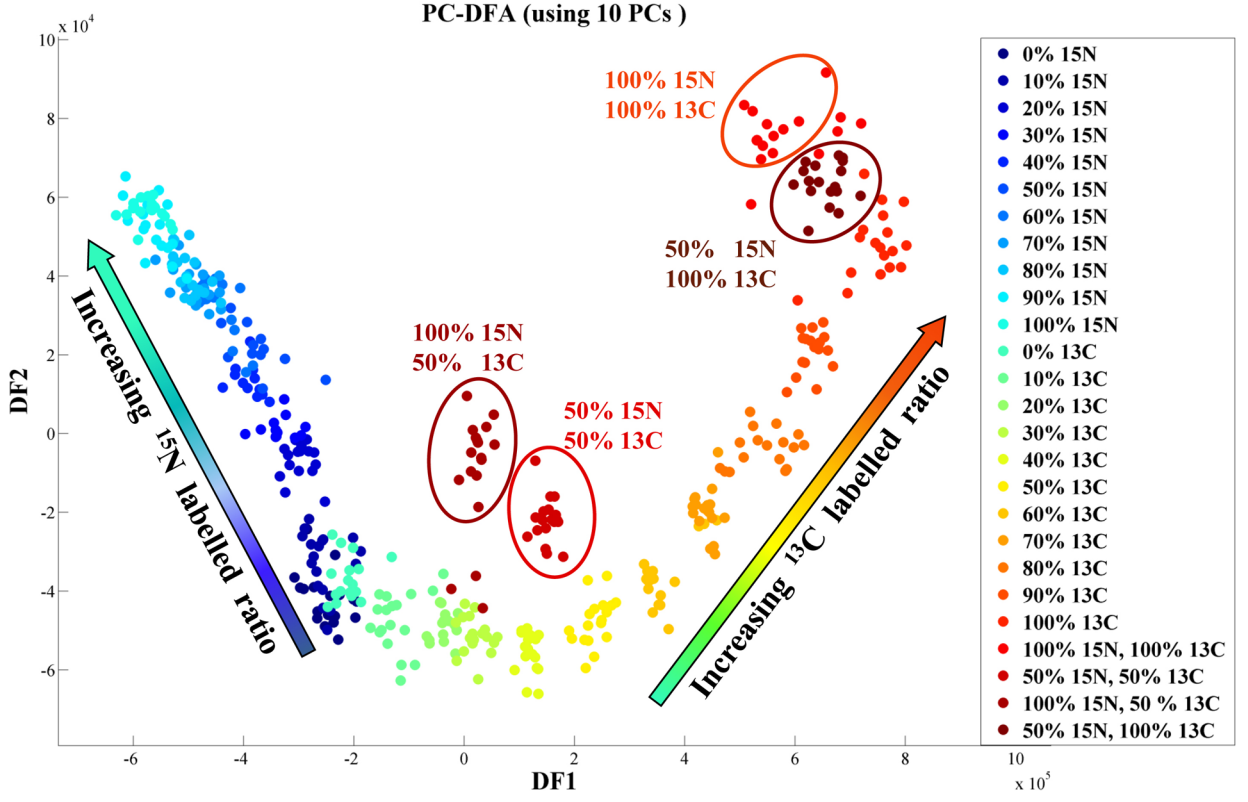

Figure 4. PC-DFA scores plot of all preprocessed Raman spectra collected from *E. coli* cells grown on minimal medium with different ratios and combinations of ^{13}C/^{12}C glucose and ^{15}N/^{14}N ammonium chloride. The arrows indicate the increasing ratio of different isotopically labeled substrates.

(Renishaw Plc., Gloucestershire, U.K.) equipped with a 785 nm diode laser and air-cooled CCD detector. All spectra were acquired using the laser power adjusted on the sample to ∼30 mW, 10 s exposure time, three accumulations, and 600 l/mm grating resulting in a spectral resolution of 6 cm^{-1}. Instrument control and data capture were achieved using the GRAMS WiRE

DOI: 10.1021/acs.analchem.5b00892
Anal. Chem. 2015, 87, 4578−4586

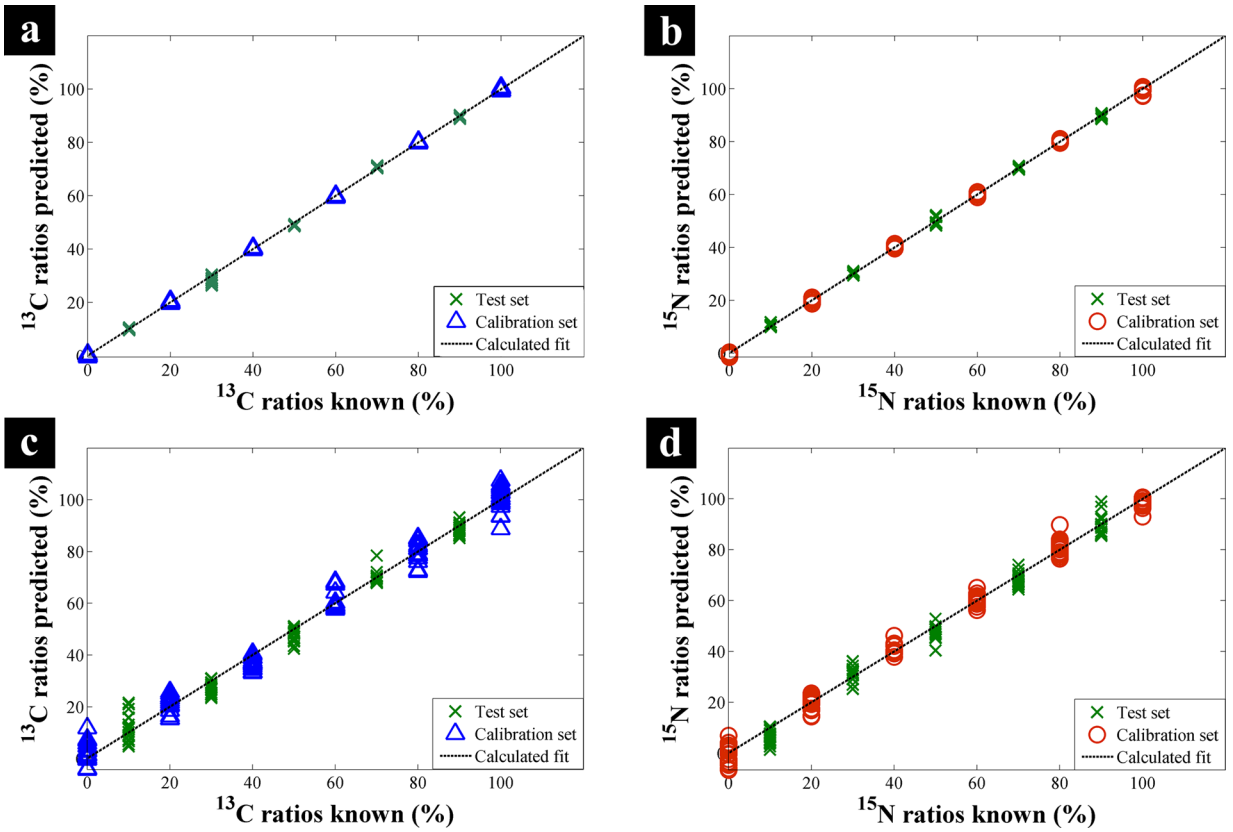

Figure 5. Plots show separate PLSR models, generated using the FT-IR (a, b) and Raman (c, d) calibration data sets, which were used for quantitative prediction of the ratio of ^{13}C and ^{15}N in the test sets. The test sets for each of the models are presented as green crosses, while the blue triangles and red circles represent the calibration sets for the ^{13}C and ^{15}N PLSR models, respectively.

3.4 software (Galactic Industries Corp. Salem, NH), and a 50× magnifying objective was used for sample observation.

For single cell Raman analysis, washed cell solutions were diluted using sterile deionized water to reduce cell density to single cell level. Samples were spotted (2 μL) onto CaF_2 disks and air-dried in a desiccator. Single cell Raman spectra were obtained using a 50× magnifying objective and a 532 nm diode laser equipped on a Renishaw InVia confocal Raman microscope, with 20 s exposure time, three accumulations, 2400 l/mm grating, and the laser power of 10 mW focused of single cells. With this set up, the approximate voxel diameter was <1 μm (equivalent to the width of the *E. coli* cells), and the voxel volume was about 1 pL. Three different *E. coli* cells were randomly selected and analyzed for each condition. All obtained Raman spectra were baseline corrected, scaled (EMSC),[34] and smoothed using a triangular sliding average.[35]

Data Analysis. All collected FT-IR and Raman spectra were processed using MATLAB software version 2011a (The Mathworks Inc., Natwick, U.S.A.). The collected multivariate data sets were investigated by employing principal component analysis (PCA).[36] Raman data were further examined by principal component-discriminant function analysis (PC-DFA) approach (Gromski *et al.*, in press[37]), a semisupervised classification method which functions by minimizing within group variance while maximizing between group variance;[38] this is considered semisupervised as the group structure here were the biological replicates rather than the type or level of the varying labeled substrates used for growth.[39]

Partial least-squares regression (PLSR) analysis[40,41] was also employed to generate separate models for predicting the percentage ratios of ^{13}C and ^{15}N for the Raman and FT-IR community-analysis data sets. The PLSR models were built using the FT-IR and Raman data from six different labeling conditions (0, 20, 40, 60, 80, and 100%, ^{13}C or ^{15}N), following methods as described previously.[22,42] Using the generated models, the ratios of ^{13}C or ^{15}N in the remaining data sets (10, 30, 50, 70, and 90%) were predicted.

RESULTS AND DISCUSSION

During the past decade the application of SIP combined with Raman microspectroscopy has attracted a lot of attention for identification, differentiation and characterization of microbially mediated processes.[28,43] However, to date, all studies have focused on isotope labeling where the organism is cultured on fully labeled substrates. While obviously useful and has shown that "SIP-Raman" is a valuable tool for discrimination of labeled bacteria, this does not mimic the environment where there is competition for resources. Therefore, this study is novel as it

Table 1. Comparison of FT-IR and Raman PLSR Models for Their Reproducibility and Accuracy of Predicting the Ratio of the Isotopic Labels

analytical method	isotope	factors	Q^2	R^2	RMSEP	RMSECV
FT-IR	^{13}C	9	0.9981	0.9999	0.3075	0.9810
FT-IR	^{15}N	3	0.9988	0.9995	0.7832	0.7658
Raman	^{13}C	2	0.9357	0.9857	4.0994	5.5323
Raman	^{15}N	6	0.9691	0.9932	2.8855	4.0654

DOI: 10.1021/acs.analchem.5b00892
Anal. Chem. 2015, 87, 4578−4586

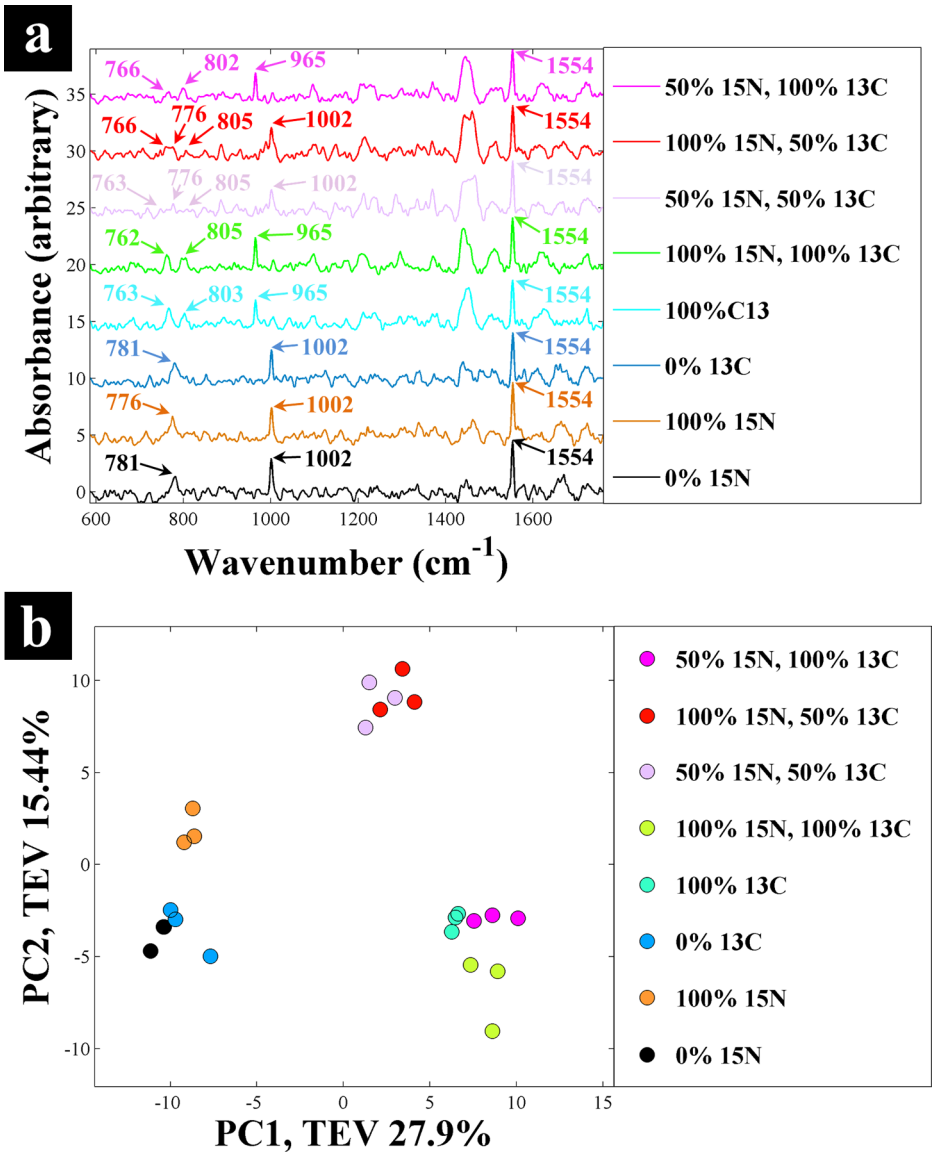

Figure 6. Differentiation of *E. coli* cells incubated with various combinations of isotopically labeled glucose (^{13}C) and ammonium chloride (^{15}N), at single cell level. (a) Raman spectra of single cells grown under various conditions—spectra are off set for easy of viewing, (b) corresponding PCA scores plot of the Raman spectra collected from three single cells of each conditions.

focused on growing *E. coli* cells on *different* ratios of isotopically labeled carbon and nitrogen sources to establish the potential of combining SIP with Raman microspectroscopy and FT-IR as metabolic fingerprinting tools for *quantitative* differentiation and labeling of bacterial cells. We note that as the final concentrations of the carbon or nitrogen sources does not change, but that the ratios of $^{13}C/^{12}C$ and $^{15}N/^{14}N$ do, the cells are in fact phenotypically identical (and bacterial growth curves (Figure S1) shows this to be the case), but their isotope content as a function of metabolism will be different.

FT-IR Metabolic Fingerprints. Figure 1 illustrates the FT-IR spectra of *E. coli* cells grown on labeled (^{13}C, ^{15}N) and unlabeled (^{12}C, ^{14}N) carbon and nitrogen sources, demonstrating various spectral shifts due to an increased reduced mass (eqs 1 and 2) resulting from the incorporation of isotopically labeled molecules by the cells. To investigate the effects of reduced mass on the detected vibrational frequencies further, eq 3 was used (conversion of eqs 1 and 2) to calculate the percentage error of the detected wavenumbers in comparison to their theoretically calculated reduced mass.

The frequency of the bond vibrations are described by eq 1:[44]

$$\bar{\nu} = \frac{1}{2\pi c}\sqrt{\frac{k}{\mu}} \tag{1}$$

where $\bar{\nu}$ is the frequency of vibration (cm^{-1}), c is the speed of light (ms^{-1}), k is the force constant of a diatomic bond (Nm^{-1}), and μ is the reduced mass given by eq 2:

$$\mu = \frac{m_1 m_2}{m_1 + m_2} \tag{2}$$

where m_1 and m_2 are the masses of the two atoms forming a bond.

$$\frac{\bar{\nu}_1}{\bar{\nu}_2} = \frac{\mu_2}{\mu_1} \tag{3}$$

where $\bar{\nu}_1$ and $\bar{\nu}_2$ are the wavenumbers of particular peaks in the FT-IR spectra of unlabeled and labeled samples, and μ_1 and μ_2

DOI: 10.1021/acs.analchem.5b00892
Anal. Chem. 2015, 87, 4578−4586

are the calculated reduced mass of unlabeled and labeled samples, respectively. The results of the calculations are presented on Figure 1 for bands that exhibited major shifts.

Figure 1a suggests that the two main FT-IR spectral bands affected by the consumption of ^{13}C-glucose are the 1655 and 1547 cm^{-1} peaks corresponding to amide I (C═O stretching vibrations) and amide II bands (combination of C−N stretching and N−H bending), respectively. Moreover, various other bands with lower intensities (Figure 1b,c) also displayed shifts due to the incorporation of ^{13}C atoms. By contrast, the detected amide I (Figure 1d) and other lower intensity bands (Figure 1e,f) in the FT-IR spectra of cells grown with ^{15}N-ammonium chloride did not display any significant shifts, while amide II band illustrated a shift of −15 cm^{-1} due to the incorporation of ^{15}N atoms (Figure 1d). This observation is perhaps not surprising, considering it is commonly accepted that nitrogen atoms do not contribute toward amide I band, while amide II vibrations are due to the C−N stretching and N−H bending of peptides and proteins.[45] Details of the affected FT-IR bands and their corresponding assignments are provided in Table S2. Individual principal component analysis (PCA) scores plots of the FT-IR data collected from cells with varying ratios of ^{15}N-ammonium chloride (Figure S2a) or ^{13}C-glucose (Figure S2b), demonstrated a concentration-dependent clustering pattern, and their corresponding PC1 loadings plots (Figure S2c) confirmed the above findings by revealing amide I and amide II bands as the most significant variables affected by the different isotopic substitution conditions.

This isotope-dependent vibrational frequency effect is even more apparent in Figure 1g, through the comparison of FT-IR spectra from *E. coli* cells grown with different combinations of labeled and unlabeled C and N substrates. The amide II band (C−N, N−H) of cells grown with unlabeled ammonium chloride and glucose (0% ^{15}N, 0% ^{13}C) is detected at 1545 cm^{-1}, while the incorporation of labeled ammonium chloride (100% ^{15}N, 0% ^{13}C) or glucose (0% ^{15}N, 100% ^{13}C) caused a shift to lower wavenumbers, around 1530 and 1535 cm^{-1}, respectively. However, this shift was even higher (1520 cm^{-1}) for the cells grown using both labeled compounds (100% ^{15}N, 100% ^{13}C; Figure 1g). Similar to amide II, the amide III band (C−N, N−H; 1240 cm^{-1}) also displayed a shift to lower wavenumbers upon ^{13}C (1236 cm^{-1}) or ^{15}N (1236 cm^{-1}) incorporation, while exhibited the highest shift when both isotopes were incorporated simultaneously (1232 cm^{-1}) (Figure 1g). The above observation can be attributed to the combined effects of the incorporation of heavier atoms (^{13}C and/or ^{15}N) on the C−N and N−H vibrational frequencies, which contribute toward the amide II and III spectral bands.

To examine the effects of ^{13}C and ^{15}N incorporation on the FT-IR spectra further, all FT-IR data were subjected to PCA to identify any specific isotope-mediated metabolic trends linked with the labeling process. The PCA scores plot (Figure 2) displayed a clear isotopic ratio-dependent separation between spectra of cells grown with different ratios of ^{13}C/^{12}C and ^{15}N/^{14}N, while those of cells grown with different combinations of both isotopes were also separated accordingly.

Figure 2 shows that the first principal component (PC1), which is the most important feature, accounts for 90.8% total explained variance (TEV) which largely accounts for the ^{13}C/^{12}C-glucose effects. By contrast PC2, which only accounts for 6.1% TEV, demonstrates a less significant effect on the spectra by the ^{15}N incorporation into the cells. This is perhaps not surprising considering the relatively higher number of carbon-related vibrational bands within the mid-IR region and also the relatively higher bacterial carbon content in comparison to nitrogen content (C/N ratio 5.9 ± 1.1).[46,47]

Raman Metabolic Fingerprints. To complement the FT-IR analysis and perhaps explore the tantalising possibility of single bacterium cell analysis, all samples were also examined by Raman microspectroscopy. It is clear in Figure 3a,b that some of the bands detected in the Raman spectra are shifted to lower wavenumbers due to the consumption of the heavier isotopes of ^{13}C-glucose and ^{15}N-ammonium chloride by the cells. A summarized list of these major Raman band shifts are provided in Table S3.

The peak at 783 cm^{-1} (Figure 3a,b) assigned to stretching vibrations in DNA and RNA bases (cytosine and uracil)[48,49] was affected by both ^{13}C and ^{15}N incorporation and exhibited a shift to lower wavenumbers of 769 and 778 cm^{-1} respectively. Similarly, the peaks at 1250 cm^{-1}, 1336 and 1574 cm^{-1}, ascribed to amide III,[49] adenine,[50,51] and nucleic acids,[19] respectively, were also clearly affected under both isotopic substitutions (Figure 3a,b).

By contrast, the peaks at 1003 and 1659 cm^{-1} (Figure 3a), ascribed to phenylalanine,[52] unsaturated lipids, and amide I,[53] respectively, displayed a shift to lower wavenumbers only under ^{13}C substitution and were not significantly affected by ^{15}N incorporation. This could be explained by the ^{13}C substitution effect on C−H in-plane and C−C aromatic ring breathing of the phenylalanine peak at 1003 cm^{-1},[54] and similarly on C═O stretching of amide I. However, since nitrogen atoms do not contribute to any of the above peaks, these peaks were unaffected under the examined ^{15}N substitution conditions. Similar to the PCA results of FT-IR spectral data (Figure S2), the individual PC-DFA scores plots of the Raman data (Figure S3) also demonstrated isotopic and concentration-dependent clustering patterns, while their corresponding DF1 loadings plots confirmed these findings.

All collected Raman spectra were combined and investigated by PC-DFA to identify any specific separation and clustering patterns resulting from the isotopic incorporation. PC-DFA scores plot of these Raman data (Figure 4) exhibited similar trends to the PCA scores plot of the FT-IR data, by displaying a clear separation between ^{15}N and ^{13}C substituted conditions.

By contrast to the FT-IR data (Figure 2), the Raman spectra of cells grown with combinations of both ^{13}C and ^{15}N exhibited a different pattern (Figure 4), which appeared to be mainly dominated by the ratio of ^{13}C rather than both ^{15}N isotopes. This is likely to be due to the major contribution of carbon atoms in the Raman spectra and, in particular, those from phenylalanine (benzene ring breathing mode at 1003 cm^{-1}) and amide I (C═O at 1659 cm^{-1}).

Since an isotopic concentration-dependent clustering pattern was illustrated by the PCA (Figure 2) and PC-DFA (Figure 4) of the FT-IR and Raman data sets, respectively, a partial least-squares regression (PLSR) algorithm was employed to generate separate models for each of the isotopically varied conditions (^{13}C and ^{15}N). The quantitative models (Figure 5) were generated and calibrated using the FT-IR and Raman data sets from six of the labeling conditions, as described in the methods section, and used for prediction of ^{13}C or ^{15}N ratios in the data sets of the remaining five conditions. While the PLSR models of both FT-IR (Figure 5a,b) and Raman (Figure 5c,d) data sets demonstrated high prediction accuracy with very low root-mean-square error of prediction (RMSEP) and root-mean-square error

DOI: 10.1021/acs.analchem.5b00892
Anal. Chem. 2015, 87, 4578−4586

of cross validation (RMSECV; Table 1), the PLSR models generated based on the collected FT-IR data demonstrated higher reproducibility and accuracy compared to the Raman models (Table 1).

Raman Fingerprint of Single Cells. Having established that there were clear quantitative isotope differences in these cells, as assessed by Raman spectroscopy, we attempted to examine the effects of isotopic substitutions at single cell level. Initial experiments established that all samples needed to be washed with sterile deionized water to avoid any salt crystal formation interfering with the Raman measurements (data not shown). As described in the materials and methods we optimized the deposition of the bacteria so that in the field of view there were isolated bacterial cells. Raman spectra of single *E. coli* cells were collected from three different cells for each of the labelling conditions. Figure 6a shows typical single-cell Raman spectra which also clearly display shifts to lower wavenumbers at several peaks, suggesting that the incorporation of the isotopically labeled compounds by these cells can be assessed at the single cell level.

It is also evident from these single-cell Raman spectra (Figure 6a) that they were all of much lower intensities compared to the spectra from the bulk bacterial samples. This is to be expected as the voxel volume collected was about 1 pL and the mass of a typical *E. coli* bacterium is just 665 fg.[55] Notwithstanding, the main detected peaks affected by the isotopic substitutions were consistent. The peak at 1002 cm^{-1} attributed to phenylalanine was only affected under ^{13}C substitution conditions, moving to lower wavenumbers at around 965 cm^{-1}, while it displayed no changes upon ^{15}N incorporation (Figure 6a). In addition, the peak detected at 781 cm^{-1} assigned to cytosine and uracil[48] was affected by both ^{13}C and ^{15}N substitutions, moving to lower wavenumbers at around 763 and 776 cm^{-1} respectively, which were consistent with previous studies[12,28,56] and our data reported in Table S3. The peak at 1554 cm^{-1} ascribed to the calcium fluoride disc, is also seen and is unavoidable due to the very small sample collection volume. Fortunately, it can be used as a reference peak to check for any instrumental drifts and variations.

In order to assess the reproducibility of these single cell Raman spectra they were subjected to PCA. Figure 6b shows excellent reproducibility and can be used to identify the overall effects of the isotopic substitutions. Raman spectra of unlabeled cells clustered together (Figure 6b, blue and black circles) and away from all other conditions. While ^{15}N-substituted samples were separated according to PC2 (TEV of 15.44%), and ^{13}C labeled samples clustered away from the ^{12}C and ^{14}N samples based on PC1 (TEV of 27.9%). However, as observed for the bulk biomass analysis (Figure 4), samples with different combinations of both of the heavy isotopes were dominated by the effect of ^{13}C ratio on the clustering pattern of the single cell Raman data (Figure 6b).

CONCLUSIONS

This study has clearly demonstrated the potential applications of Raman and FT-IR spectroscopies combined with SIP for quantitative labeling of bacterial cells, which to our knowledge has not been shown before. The unique features of the FT-IR and Raman spectra resulting from the incorporation of different isotopes allowed the quantitative characterization and differentiation of *E. coli* cells according to the ratio of the incorporated isotopes, both in individual and combined isotopic substituted conditions. We note that analyzing different ratios of both ^{13}C and ^{15}N combinations together has not been achieved before and this therefore opens up the enticing possibility of labeling bacterial cells with multiple substrates and using SIP-Raman as a powerful metabolic profiling tool for the analysis of bacterial communities.

In addition, the single-cell Raman results presented in this study further demonstrate the potential of this approach for biochemical investigation of individual cells, which combined with molecular biology tools may provide a better understanding and identification of the responsible communities involved in various microbially mediated bioprocesses (e.g., environmental, medical, and veterinarian).

ASSOCIATED CONTENT

Supporting Information

Additional analytical details. This material is available free of charge via the Internet at http://pubs.acs.org.

AUTHOR INFORMATION

Corresponding Author

*E-mail: roy.goodacre@manchester.ac.uk. Tel.: 0161 306-4480.

Author Contributions

†These authors have contributed equally to this publication (H.M. and M.C.).

Notes

The authors declare no competing financial interest.

ACKNOWLEDGMENTS

This work was supported by a UK BBSRC Ph.D. Studentship Grant for H.M. (ref: BB/H015868/1). M.C. is funded by the Copperbelt University, and A.S. is supported by the Umm Al-Qura University. R.G. is also grateful to BBSRC for financial support and, in particular, for Raman microscopy (BB/L014823/1).

REFERENCES

(1) Houtzager, H. L. *Eur. J. Obstet. Gynecol. Reprod. Biol.* **1983**, *15*, 199−203.
(2) Lankadurai, B. P.; Nagato, E. G.; Simpson, M. J. *Environ. Rev.* **2013**, *21*, 180−205.
(3) Bundy, J. G.; Davey, M. P.; Viant, M. R. *Metabolomics* **2009**, *5*, 3−21.
(4) Amann, R. I.; Ludwig, W.; Schleifer, K. H. *Microbiol. Rev.* **1995**, *59*, 143−169.
(5) Handelsman, J. *Microbiol. Mol. Biol. Rev.* **2004**, *68*, 669−685.
(6) Daniel, R. *Nat. Rev. Microbiol.* **2005**, *3*, 470−478.
(7) Tringe, S. G.; von Mering, C.; Kobayashi, A.; Salamov, A. A.; Chen, K.; Chang, H. W.; Podar, M.; Short, J. M.; Mathur, E. J.; Detter, J. C.; Bork, P.; Hugenholtz, P.; Rubin, E. M. *Science* **2005**, *308*, 554−557.
(8) Xu, J. P. *Mol. Ecol.* **2006**, *15*, 1713−1731.
(9) Parks, D. H.; Beiko, R. G. *Bioinformatics* **2010**, *26*, 715−721.
(10) Huang, W. E.; Bailey, M. J.; Thompson, I. P.; Whiteley, A. S.; Spiers, A. J. *Mol. Ecol.* **2007**, *53*, 414−425.
(11) Huang, W. E.; Griffiths, R. I.; Thompson, I. P.; Bailey, M. J.; Whiteley, A. S. *Anal. Chem.* **2004**, *76*, 4452−4458.
(12) Wang, Y.; Ji, Y.; Wharfe, E. S.; Meadows, R. S.; March, P.; Goodacre, R.; Xu, J.; Huang, W. E. *Anal. Chem.* **2013**, *85*, 10697−10701.
(13) Fiehn, O. *Plant Mol. Biol.* **2002**, *48*, 155−171.
(14) Goodacre, R. *Metabolomics* **2005**, *1*, 1−2.
(15) Su, C.; Lei, L.; Duan, Y.; Zhang, K.-Q.; Yang, J. *Appl. Microbiol. Biotechnol.* **2012**, *93*, 993−1003.
(16) Huang, W. E.; Li, M.; Jarvis, R. M.; Goodacre, R.; Banwart, S. A. In *Advances in Applied Microbiology*; Allen, I. L., Sima, S., Geoffrey, M. G., Eds.; Academic Press: New York, 2010; pp 153−186.
(17) Ellis, D. I.; Brewster, V. L.; Dunn, W. B.; Allwood, J. W.; Golovanov, A. P.; Goodacre, R. *Chem. Soc. Rev.* **2012**, *41*, 5706−5727.

DOI: 10.1021/acs.analchem.5b00892
Anal. Chem. 2015, 87, 4578−4586

(18) Ellis, D.; Harrigan, G.; Goodacre, R. In *Metabolic Profiling: Its Role in Biomarker Discovery and Gene Function Analysis*; Harrigan, G., Goodacre, R., Eds.; Springer: New York, 2003; pp 111−124.
(19) Maquelin, K.; Kirschner, C.; Choo-Smith, L. P.; van den Braak, N.; Endtz, H. P.; Naumann, D.; Puppels, G. J. *J. Microbiol. Methods.* **2002**, *51*, 255−271.
(20) Goodacre, R.; Timmins, é. M.; Burton, R.; Kaderbhai, N.; Woodward, A. M.; Kell, D. B.; Rooney, P. J. *Microbiology* **1998**, *144*, 1157−1170.
(21) Suci, P. A.; Mittelman, M. W.; Yu, F. P.; Geesey, G. G. *Antimicrob. Agents Chemother.* **1994**, *38*, 2125−2133.
(22) Nicolaou, N.; Xu, Y.; Goodacre, R. *Anal. Chem.* **2011**, *83*, 5681−5687.
(23) Ellis, D. I.; Broadhurst, D.; Kell, D. B.; Rowland, J. J.; Goodacre, R. *Appl. Environ. Microbiol.* **2002**, *68*, 2822−2828.
(24) Wang, H.; Hollywood, K.; Jarvis, R. M.; Lloyd, J. R.; Goodacre, R. *Appl. Environ. Microbiol.* **2010**, *76*, 6266−6276.
(25) Zhao, H.; Parry, R. L.; Ellis, D. I.; Griffith, G. W.; Goodacre, R. *Vib. Spectrosc.* **2006**, *40*, 213−218.
(26) Muhamadali, H.; Xu, Y.; Ellis, D. I.; Allwood, J. W.; Rattray, N. J. W.; Correa, E.; Alrabiah, H.; Lloyd, J. R.; Goodacre, R. *Appl. Environ. Microbiol.* **2015**, in press (DOI: 10.1128/AEM.00294-15).
(27) Smith, B. C. *Fundamentals of Fourier Transform Infrared Spectroscopy*; CRC Press: Boca Raton, FL, 2011.
(28) Huang, W. E.; Stoecker, K.; Griffiths, R.; Newbold, L.; Daims, H.; Whiteley, A. S.; Wagner, M. *Environ. Microbiol.* **2007**, *9*, 1878−1889.
(29) Huang, W. E.; Ferguson, A.; Singer, A. C.; Lawson, K.; Thompson, I. P.; Kalin, R. M.; Larkin, M. J.; Bailey, M. J.; Whiteley, A. S. *Appl. Environ. Microbiol.* **2009**, *75*, 234−241.
(30) Li, M.; Canniffe, D. P.; Jackson, P. J.; Davison, P. A.; FitzGerald, S.; Dickman, M. J.; Burgess, J. G.; Hunter, C. N.; Huang, W. E. *ISME J.* **2012**, *6*, 875−885.
(31) Boschker, H. T. S.; Nold, S. C.; Wellsbury, P.; Bos, D.; de Graaf, W.; Pel, R.; Parkes, R. J.; Cappenberg, T. E. *Nature* **1998**, *392*, 801−805.
(32) Huang, W. E.; Wang, H.; Zheng, H. J.; Huang, L. F.; Singer, A. C.; Thompson, I.; Whiteley, A. S. *Environ. Microbiol.* **2005**, *7*, 1339−1348.
(33) Winder, C. L.; Gordon, S. V.; Dale, J.; Hewinson, R. G.; Goodacre, R. *Microbiology* **2006**, *152*, 2757−2765.
(34) Martens, H.; Nielsen, J. P.; Engelsen, S. B. *Anal. Chem.* **2003**, *75*, 394−404.
(35) Brereton, R. G. *Chemometrics: Data Analysis for the Laboratory and Chemical Plant*; Wiley: West Sussex, 2005.
(36) Wold, S.; Esbensen, K.; Geladi, P. *Chemom. Intell. Lab. Syst.* **1987**, *2*, 37−52.
(37) Gromski, P. S.; Muhamadali, H.; Ellis, D. I.; Xu, Y.; Correa, E.; Turner, M. L.; Goodacre, R. *Anal. Chim. Acta* **2015**, in press (DOI: 10.1016/j.aca.2015.02.012).
(38) Macfie, H. J. H.; Gutteridge, C. S.; Norris, J. R. J. *Gen. Microbiol.* **1978**, *104*, 67−74.
(39) Goodacre, R.; Rooney, P. J.; Kell, D. B. In *Infrared Spectroscopy: New Tool in Medicine*; SPIE: 1998; pp 220−229.
(40) Geladi, P.; Kowalski, B. R. *Anal. Chim. Acta* **1986**, *185*, 1−17.
(41) Martens, H.; Naes, T. *Multivariate Calibration*; Wiley: New York, 1992.
(42) Nicolaou, N.; Xu, Y.; Goodacre, R. J. *Dairy Sci.* **2010**, *93*, 5651−5660.
(43) Wagner, M. *Annu. Rev. Microbiol.* **2009**, *63*, 411−429.
(44) *Infrared and Raman Spectroscopy*; Larkin, P., Ed.; Elsevier: Oxford, 2011; pp 7−25.
(45) Patel, S. A.; Currie, F.; Thakker, N.; Goodacre, R. *Analyst* **2008**, *133*, 1707−1713.
(46) Nagata, T. *Appl. Environ. Microbiol.* **1986**, *52*, 28−32.
(47) Fukuda, R.; Ogawa, H.; Nagata, T.; Koike, I. *Appl. Environ. Microbiol.* **1998**, *64*, 3352−3358.
(48) Maquelin, K.; Choo-Smith, L. P.; Endtz, H. P.; Bruining, H. A.; Puppels, G. J. J. *Clin. Microbiol.* **2002**, *40*, 594−600.
(49) Naumann, D. *Appl. Spectrosc. Rev.* **2001**, *36*, 239−298.
(50) Hering, K.; Cialla, D.; Ackermann, K.; Doerfer, T.; Moeller, R.; Schneidewind, H.; Mattheis, R.; Fritzsche, W.; Roesch, P.; Popp, J. *Anal. Bioanal. Chem.* **2008**, *390*, 113−124.
(51) Uzunbajakava, N.; Lenferink, A.; Kraan, Y.; Volokhina, E.; Vrensen, G.; Greve, J.; Otto, C. *Biophys. J.* **2003**, *84*, 3968−3981.
(52) Harz, M.; Rosch, P.; Peschke, K. D.; Ronneberger, O.; Burkhardt, H.; Popp, J. *Analyst* **2005**, *130*, 1543−1550.
(53) van Manen, H. J.; Kraan, Y. M.; Roos, D.; Otto, C. *Proc. Natl. Acad. Sci. U.S.A.* **2005**, *102*, 10159−10164.
(54) Williams, A. C.; Edwards, H. G. M. J. *Raman Spectrosc.* **1994**, *25*, 673−677.
(55) Ramos, D.; Tamayo, J.; Mertens, J.; Calleja, M.; Zaballos, A. J. *Appl. Phys.* **2006**, *100*, 106105.
(56) Li, M.; Huang, W. E.; Gibson, C. M.; Fowler, P. W.; Jousset, A. *Anal. Chem.* **2012**, *85*, 1642−1649.

DOI: 10.1021/acs.analchem.5b00892
Anal. Chem. 2015, 87, 4578−4586